

Article

Discretization Approach for the Homogenization of Three-Dimensional Solid-Solid Phononic Crystals in the Quasi-Static Limit: Density and Elastic Moduli

J. Flores Méndez ^{1,2,*}, A. C. Pinón Reyes ^{1,2}, Aurelio H. Heredia Jiménez ³, Roberto C. Ambrosio Lázaro ¹, A. Morales-Sánchez ⁴, M. Moreno Moreno ⁴, J. A. Luna-López ¹, F. Severiano Carrillo ⁵ and M. A. Meraz Melo ^{2,*}

- ¹ Facultad de Electrónica, Benemérita Universidad Autónoma de Puebla, Blvd. Valsequillo y Esquina, Av. San Claudio s/n, Col. San Manuel, Puebla C.P. 72570, Mexico; ana.pinon@alumno.buap.mx (A.C.P.R.); roberto.ambrosio@correo.buap.mx (R.C.A.L.); jose.luna@correo.buap.mx (J.A.L.-L.)
- ² Tecnológico Nacional de México/I.T. Puebla-División de Estudios de Posgrado e Investigación, Av. Tecnológico No. 420, Maravillas, Puebla C.P. 72220, Mexico
- ³ Facultad de Electrónica, UPAEP, 21 sur No. 1103, Barrio de Santiago, Puebla C.P. 72410, Mexico; aureliohoracio.heredia@upaep.mx
- ⁴ Instituto Nacional de Astrofísica, Óptica y Electrónica, Luis Enrique Erro No. 1, Sta. Ma. Tonantzintla, Puebla C.P. 72840, Mexico; alfredom@inaoep.mx (A.M.-S.); mmoreno@inaoep.mx (M.M.M.)
- ⁵ CONACYT, Av. Insurgentes Sur 1582, Col. Crédito Constructor, Del. Benito Juárez, Mexico City C.P. 03940, Mexico; fseveriano@conacyt.mx
- * Correspondence: javier.floresme@correo.buap.mx (J.F.M.); marco.meraz@puebla.tecnm.mx (M.A.M.M.); Tel.: +52-222-3160-085 (J.F.M.); +52-222-2655-646 (M.A.M.M.)



Citation: Flores Méndez, J.; Pinón Reyes, A.C.; Heredia Jiménez, A.H.; Ambrosio Lázaro, R.C.; Morales-Sánchez, A.; Moreno Moreno, M.; Luna-López, J.A.; Severiano Carrillo, F.; Meraz Melo, M.A. Discretization Approach for the Homogenization of Three-Dimensional Solid-Solid Phononic Crystals in the Quasi-Static Limit: Density and Elastic Moduli. *Appl. Sci.* **2022**, *12*, 2987. <https://doi.org/10.3390/app12062987>

Academic Editor: Tatjana Gric

Received: 25 February 2022

Accepted: 11 March 2022

Published: 15 March 2022

Publisher's Note: MDPI stays neutral with regard to jurisdictional claims in published maps and institutional affiliations.

Abstract: With the application of a homogenization theory, based on the Fourier formalism (which provides efficient and exact formulas by which to determine all the components of the effective stiffness and mass density tensors, valid in the regime of large wavelengths), a new approach to calculate the effective quasi-static response in three-dimensional solid-solid phononic crystals is reported. The formulas derived in this work for calculating the effective elastic parameters show a dependence, in terms of summations over the vectors, of the reciprocal lattice by the discretization of the volume of the inclusion in small parts (e.g., small cubes), to obtain a system of equations from which we define the effective response. In particular, we present the numerical results calculated for several cubic lattices with solid constituents and different shapes of inclusions in the unit cell versus the filling fraction, as well as for fixed values of it. By this means, we analyzed the effect of the type of Bravais lattice of the materials, and the geometry of the inclusions that constitute the three-dimensional phononic array, on the resulting effective anisotropy. Finally, our theory confirms other well-known results with previous homogenization theories as a particular case study. In this regard, the examples and results shown here can be useful for the design of metamaterials with predetermined elastic properties.

Keywords: phononic crystal; homogenization theory; effective parameters; metamaterial



Copyright: © 2022 by the authors. Licensee MDPI, Basel, Switzerland. This article is an open access article distributed under the terms and conditions of the Creative Commons Attribution (CC BY) license (<https://creativecommons.org/licenses/by/4.0/>).

1. Introduction

The calculation of the effective elastic parameters or effective propagation velocities of elastic waves in composite materials is a classic problem of great interest for researchers in this field over the past few decades. Most of the previous approaches establish the upper and lower limits [1,2] based on the crystalline symmetry of the structure or by effective medium theories [3,4]. Kushwaha et al. [5] used the term “phononic crystals” in their study of the plane waves method in periodic composites. The plane wave expansion method is an efficient approach that allows calculating the effective speed of sound through a phononic crystal, where the dispersion relation is linear [6–10], i.e., within the quasi-static

limit ($\omega, k \rightarrow 0$). Within the context of the quasi-static regime, it is established that when the wavelength of the acoustic waves is much larger than the lattice constant of the respective crystals, these artificial compounds can be modeled as homogeneous media with effective physical parameters. Other approaches relate the effective density and the elastic constants with Christoffel's equation to calculate the propagation velocities of the elastic waves, according to the different directions of the principal axes [6,11,12]. At the long-wavelength limit, the effective density for solid-solid composites is isotropic-linear and depends on the filling fraction of the inclusion [3]. This condition is different for composite structures with a fluid matrix, which gives rise to acoustic metamaterials characterized by an anisotropic effective mass density [12–16]. In this context of the study of elastic (acoustic) waves, propagating in solid-solid (solid-liquid) phononic periodic structures, we can cite the recent work by [17]. In that work, the authors propose a homogenization theory on the long-wavelength limit to estimate the effective velocities as a function of the direction of propagation of the elastic wave, within the phononic periodic structure of the sonic or elastic type. Through a variational technique and implementation of the finite element method, they determine the effective anisotropy of the phononic crystal and generalize the Christoffel equation in this way for different designs of one-dimensional, two-dimensional, and three-dimensional structures. They also study the anisotropy of the acoustic/elastic waves propagation in these relevant cases. Among all types of phononic structures, there are the so-called metamaterials. Extending this concept to the case of acoustic metamaterials, from the point of view of a homogeneous medium, it is required that both the effective density and bulk modulus be simultaneously negative; with these characteristics, the waves can propagate through the medium with an index negative refraction, whose principal effect is refracting the waves negatively, hence, acting as a superlens (see [18,19] and its references). More recently, a growing interest has developed in the design, manufacture, and study of the mechanical properties of chiral elastic metamaterials. Different two-dimensional and three-dimensional geometries for the crystal architecture of a chiral mechanical metamaterial can be designed by using various modern additive manufacturing techniques [20–22]. To describe the physical properties of these artificial materials, various homogenization methods have been proposed that characterize their behavior as a continuous medium by means of constitutive equations (micropolar elasticity theory) [23–26]. The numerical solution of these approaches (e.g., the finite element method) allows researchers to investigate the benefits and mechanical limitations of their unusual behaviors, such as: negative Poisson's ratio (auxetics materials) [27], negative coefficient of thermal expansion [28], wave manipulation [29], bandgap features [30], impact energy absorption [31,32] or vibration attenuation [33,34]. Other important studies refer to the propagation of elastic waves along a particular direction through the design of elastic wave metamaterials since one of their main characteristics is the defect state. If these periodic structures present defects, the elastic wave will be located near a punctual defect, whereas in the case of linear defects, it will propagate along it. For example, Kuan-Xin et al. have shown numerical calculations in their recent works [35–37] to determine the crack resistance behaviors for some special frequency regions in which the effective parameters show dynamic negative values. Consequently, the elastic wave metamaterials with local resonators can demonstrate their excellent arrest properties during crack propagation.

In the past few years, in [38] a homogenization theory was proposed based on Fourier formalism, which provides efficient and exact formulas to determine all the components of the effective stiffness and mass density tensors, valid in the regime of large wavelengths. In that work, it was shown that in the quasi-static limit, two-dimensional arrangements with a rectangular lattice of water-filled holes in a solid-elastic host matrix exhibit anisotropy in the effective density and compliance tensor, denoting this metamaterial as a *metasolid*. On the other hand, in the same homogenization regime, the effective elastic response for one-dimensional and two-dimensional solid-solid phononic crystals is also calculated.

The problem of calculating the effective parameters of heterogeneous media lies in the calculation of the inversion of large matrices, principally in the case of three-dimensional

phononic structures. In developing our theory from the master equation presented in [38], this is redefined in terms of summations over the vectors of the reciprocal lattice by the discretization of the inclusion in small volumes, to establish a system of equations from which we can obtain the effective elastic response of the phononic crystal.

The purpose of this work is to highlight a new method to calculate the effective mass density and stiffness tensors for a three-dimensional solid-solid phononic crystal at the quasi-static limit. In the following sections, we first summarize the deduction of the secular equation to obtain the homogenization parameters by studying the quasi-static limit. Secondly, numerical results calculated for several cubic lattices with solid constituents and different shapes of inclusions in the unit cell, versus the filling fraction and for fixed values of it, are presented. In addition, a comparison of our results with other theories is carried out. Finally, the findings of this work are summarized.

2. General Approach to Homogenization

It was shown in the study by [38] that the elastic properties of a phonon crystal are based on the basic physical ideas of Hooke’s law and Newton’s second law. Using Voigt’s notation, the matrix-unified representation of these two laws is as follows:

$$\begin{bmatrix} 0_3 & \nabla_{3 \times 6} \\ (\nabla_{3 \times 6})^T & 0_6 \end{bmatrix} \mathbf{v}(\mathbf{r}) = \Omega A(\mathbf{r})\mathbf{v}(\mathbf{r}), \tag{1}$$

where:

$$\nabla_{3 \times 6} = \begin{pmatrix} \nabla_1 & 0 & 0 & 0 & \nabla_3 & \nabla_2 \\ 0 & \nabla_2 & 0 & \nabla_3 & 0 & \nabla_1 \\ 0 & 0 & \nabla_3 & \nabla_2 & \nabla_1 & 0 \end{pmatrix}, \tag{2}$$

$$[\mathbf{v}(\mathbf{r})]^T = (u_1, u_2, u_3, \sigma_1, \sigma_2, \sigma_3, \sigma_4, \sigma_5, \sigma_6), \tag{3}$$

$$\Omega = \begin{bmatrix} -\omega^2 I_3 & 0_{3 \times 6} \\ 0_{6 \times 3} & I_6 \end{bmatrix}. \tag{4}$$

In the above expressions, ω is the frequency, I_i and $0_{i \times j}$ are the unity and zero matrices, the order of which is indicated by the subscripts, and $[\mathbf{v}(\mathbf{r})]^T$ corresponds to the 9×9 column vector with the components of the displacement and stress vectors. The matrix $A(\mathbf{r})$ of order 9×9 is a periodic function of the coordinate \mathbf{r} and is expressed in terms of the mass density $\rho(\mathbf{r})$ and the 6×6 compliance tensor, $S(\mathbf{r})$, so this can be cast as:

$$A(\mathbf{r}) = \begin{bmatrix} \rho(\mathbf{r})I_3 & 0_{3 \times 6} \\ 0_{6 \times 3} & S(\mathbf{r}) \end{bmatrix}. \tag{5}$$

Using the previous definitions and following the homogenization methodology, based on the plane-wave expansion indicated in the study by [38], the effective tensors of the homogenized phononic crystal $\bar{\rho}_{eff}$ and \bar{S}_{eff} , as a function of the wave vector \mathbf{k} and the frequency ω , are defined by the following effective non-local response matrix:

$$A_{eff}(\mathbf{k}) = i\Omega^{-1}\{D^{-1}(\mathbf{k}; 0, 0)\}^{-1} + i\Omega^{-1} \begin{bmatrix} 0_3 & K_{3 \times 6}(\mathbf{k}) \\ (K_{3 \times 6}(\mathbf{k}))^T & 0_6 \end{bmatrix} = \begin{bmatrix} \bar{\rho}_{eff}(\mathbf{k}, \omega) & 0_{3 \times 6} \\ 0_{6 \times 3} & \bar{S}_{eff}(\mathbf{k}, \omega) \end{bmatrix}, \tag{6}$$

where the matrix elements of $K_{3 \times 6}$ are:

$$K_{3 \times 6}(\mathbf{k}) = \begin{pmatrix} k_1 & 0 & 0 & 0 & k_3 & k_2 \\ 0 & k_2 & 0 & k_3 & 0 & k_1 \\ 0 & 0 & k_3 & k_2 & k_1 & 0 \end{pmatrix}, \tag{7}$$

being $D^{-1}(\mathbf{k}; 0, 0)$, a matrix block of size 9×9 obtained from the inverse of the matrix of infinite size $D^{-1}(\mathbf{k}; \mathbf{G}, \mathbf{G}')$, such that:

$$D(\mathbf{k}; \mathbf{G}, \mathbf{G}') = - \begin{bmatrix} 0_3 & K_{3 \times 6}(\mathbf{k} + \mathbf{G}) \\ (K_{3 \times 6}(\mathbf{k} + \mathbf{G}))^T & 0_6 \end{bmatrix} \delta_{\mathbf{G}, \mathbf{G}'} - i\Omega A(\mathbf{G} - \mathbf{G}'), \quad (8)$$

with \mathbf{G} and $A(\mathbf{G} - \mathbf{G}')$ as the reciprocal lattice vector and the Fourier coefficient of the matrix $A(\mathbf{r})$, respectively.

The long-wavelength regime corresponds to the lower part of the band structure, that is, when $\mathbf{k} \rightarrow 0, \omega \rightarrow 0$. Applying this criterion to Equation (6), the $A_{eff}(\mathbf{k} \rightarrow 0, \omega \rightarrow 0)$ matrix corresponding to the quasistatic limit takes the form:

$$A_{eff}(\mathbf{k} \rightarrow 0) = i \lim_{\mathbf{k} \rightarrow 0} \Omega^{-1} \{ D^{-1}(\mathbf{k}; 0, 0) \}^{-1} = \begin{bmatrix} \bar{\rho}_{eff} & 0_{3 \times 6} \\ 0_{6 \times 3} & \bar{S}_{eff} \end{bmatrix}. \quad (9)$$

Next, we will present a rigorous approach for efficient, accurate calculation of the effective parameters of a homogenized three-dimensional phononic crystal, where the inclusion and host materials in the unit cell have the densities ρ_a and ρ_b , and elastic compliance constants S_a and S_b , respectively.

So, within this context of effective medium, to obtain $A_{eff}(\mathbf{k})$, we will determine the matrix $D^{-1}(\mathbf{k}; \mathbf{G}, \mathbf{G}')$ from the following equation:

$$\sum_{\mathbf{G}'} D(\mathbf{k}; \mathbf{G}, \mathbf{G}') D^{-1}(\mathbf{k}; \mathbf{G}', \mathbf{G}'') = I \delta_{\mathbf{G}, \mathbf{G}''}, \quad (10)$$

where the unitary matrix I is sized 9×9 . Applying the definition of $D(\mathbf{k}; \mathbf{G}, \mathbf{G}')$ indicated in (8), Equation (10) can be expressed by:

$$- \begin{bmatrix} 0_3 & K_{3 \times 6}(\mathbf{k} + \mathbf{G}) \\ (K_{3 \times 6}(\mathbf{k} + \mathbf{G}))^T & 0_6 \end{bmatrix} D^{-1}(\mathbf{k}; \mathbf{G}, \mathbf{G}'') + \frac{\Omega}{i} \sum_{\mathbf{G}'} A(\mathbf{G} - \mathbf{G}') D^{-1}(\mathbf{k}; \mathbf{G}', \mathbf{G}'') = I \delta_{\mathbf{G}, \mathbf{G}''}. \quad (11)$$

It is important to remember that the Fourier coefficients of the matrix $A(\mathbf{r})$ are given by:

$$A(\mathbf{G} - \mathbf{G}') = \begin{bmatrix} \rho_b I & 0_{3 \times 6} \\ 0_{6 \times 3} & S_b I \end{bmatrix} \delta_{\mathbf{G}, \mathbf{G}'} + \begin{bmatrix} \Delta \rho I & 0_{3 \times 6} \\ 0_{6 \times 3} & \Delta S_{6 \times 6} I \end{bmatrix} \cdot F(\mathbf{G} - \mathbf{G}'), \quad (12)$$

where $\Delta \rho = \rho_a - \rho_b$, $\Delta S = S_a - S_b$ and $F(\mathbf{G} - \mathbf{G}')$ is the form factor of the inclusion. An alternative, more simplified, expression of Equation (12) can be used by redefining the following terms:

$$A_b = \begin{bmatrix} \rho_b I & 0_{3 \times 6} \\ 0_{6 \times 3} & S_b I \end{bmatrix}, \quad (13)$$

$$\Delta A(\mathbf{G} - \mathbf{G}') = \begin{bmatrix} \Delta \rho I & 0_{3 \times 6} \\ 0_{6 \times 3} & \Delta S_{6 \times 6} I \end{bmatrix} F(\mathbf{G} - \mathbf{G}'). \quad (14)$$

By using the definition of Equation (12) in (11), and after a few manipulations, we obtain:

$$\bar{T}(\mathbf{G}) \cdot D^{-1}(\mathbf{k}; \mathbf{G}, \mathbf{G}'') + \frac{\Omega}{i} \sum_{\mathbf{G}'} \Delta A(\mathbf{G} - \mathbf{G}') D^{-1}(\mathbf{k}; \mathbf{G}', \mathbf{G}'') = I \delta_{\mathbf{G}, \mathbf{G}''}, \quad (15)$$

where:

$$\bar{T}(\mathbf{G}) = - \begin{bmatrix} 0_3 & K_{3 \times 6}(\mathbf{k} + \mathbf{G}) \\ (K_{3 \times 6}(\mathbf{k} + \mathbf{G}))^T & 0_6 \end{bmatrix} + \frac{\Omega}{i} A_b = \begin{bmatrix} -\frac{\Omega}{i} \rho_b I & -K_{3 \times 6}(\mathbf{k} + \mathbf{G}) \\ -(K_{3 \times 6}(\mathbf{k} + \mathbf{G}))^T & -\frac{\Omega}{i} S_b I \end{bmatrix} \quad (16)$$

Realizing the product of Equation (15) using the matrix $\overline{\overline{T}}^{-1}(\mathbf{G})$, we get:

$$D^{-1}(\mathbf{k}; \mathbf{G}, \mathbf{G}'') + \overline{\overline{T}}^{-1}(\mathbf{G}) \frac{\Omega}{i} \sum_{\mathbf{G}'} \Delta A(\mathbf{G} - \mathbf{G}') D^{-1}(\mathbf{k}; \mathbf{G}', \mathbf{G}'') = \overline{\overline{T}}^{-1}(\mathbf{G}) I \delta_{\mathbf{G}, \mathbf{G}'}, \quad (17)$$

where the matrix $\overline{\overline{T}}^{-1}(\mathbf{G})$, sized 9×9 , is defined as:

$$\overline{\overline{T}}^{-1}(\mathbf{G}) = \begin{bmatrix} T_{uu}^{-1} & T_{u\sigma}^{-1} \\ T_{\sigma u}^{-1} & T_{\sigma\sigma}^{-1} \end{bmatrix}. \quad (18)$$

In general, Equation (18) is solved numerically. However, in the isotropic scenario, the elements $uu, u\sigma, \sigma u$ and $\sigma\sigma$ of this matrix are defined as:

$$\overline{\overline{T}}_{uu}^{-1}(\mathbf{G}) = - \left[\frac{\overleftrightarrow{P}_T(\mathbf{k} + \mathbf{G})}{\frac{\omega^2}{i} \rho_b + i|\mathbf{k} + \mathbf{G}|^2 C_{44,b}} + \frac{\overleftrightarrow{P}_L(\mathbf{k} + \mathbf{G})}{\frac{\omega^2}{i} \rho_b + i|\mathbf{k} + \mathbf{G}|^2 C_{11,b}} \right], \quad (19)$$

$$\overline{\overline{T}}_{\sigma u}^{-1}(\mathbf{G}) = iS_b^{-1} K^T \overline{\overline{T}}_{uu}^{-1}(\mathbf{G}), \quad (20)$$

$$\overline{\overline{T}}_{u\sigma}^{-1}(\mathbf{G}) = \overline{\overline{T}}_{uu}^{-1}(\mathbf{G}) K iS_b^{-1}, \quad (21)$$

$$\overline{\overline{T}}_{\sigma\sigma}^{-1}(\mathbf{G}) = iS_b^{-1} [I_6 + K^T \overline{\overline{T}}_{uu}^{-1}(\mathbf{G}) K iS_b^{-1}], \quad (22)$$

where $\overleftrightarrow{P}_T(\mathbf{k} + \mathbf{G}) = I - \frac{(\mathbf{k} + \mathbf{G})(\mathbf{k} + \mathbf{G})}{|\mathbf{k} + \mathbf{G}|^2}$ and $\overleftrightarrow{P}_L(\mathbf{k} + \mathbf{G}) = \frac{(\mathbf{k} + \mathbf{G})(\mathbf{k} + \mathbf{G})}{|\mathbf{k} + \mathbf{G}|^2}$ correspond to the transverse and longitudinal projectors, respectively.

As can be seen in Equation (6), it is not necessary to know all the elements of $D^{-1}(\mathbf{k}; \mathbf{G}, \mathbf{G}'')$ but only the $D^{-1}(\mathbf{k} = 0; \mathbf{G}' = 0, \mathbf{G}'' = 0)$ block; therefore, when writing Equation (17) for $\mathbf{G}'' = 0$, we obtain a system of equations for the column block $D^{-1}(\mathbf{k}; \mathbf{G}, 0)$:

$$D^{-1}(\mathbf{k}; \mathbf{G}, 0) + \overline{\overline{T}}^{-1}(\mathbf{G}) \frac{\Omega}{i} \sum_{\mathbf{G}'} \Delta A(\mathbf{G} - \mathbf{G}') D^{-1}(\mathbf{k}; \mathbf{G}', 0) = \overline{\overline{T}}^{-1}(\mathbf{G}) I \delta_{\mathbf{G}, 0}, \quad (23)$$

The form factor $F(\mathbf{G})$ in Equation (14) varies very slowly when the filling fraction f (ratio between the volume occupied by the inclusion within the unit cell with respect to the total volume of the cell) is too small (small inclusions), being constant for large values of $|\mathbf{G}|$ ($|\mathbf{G}| \sim 1/r \gg 1/a$; r and a are the characteristic size of the inclusion and the lattice constant, respectively). To determine the block of the matrix $D^{-1}(\mathbf{k}; 0, 0)$, the matrix $\Delta A(\mathbf{G} - \mathbf{G}')$ in Equation (17) can be replaced by $\Delta A(-\mathbf{G}')$ (with $F(\mathbf{G} - \mathbf{G}') \rightarrow F(-\mathbf{G}')$) because the contrast for \mathbf{G} close to the origin is negligible. This consideration allows us to analytically calculate the column block $D^{-1}(\mathbf{k}; \mathbf{G}, 0)$. In this way, we can see that Equation (23) takes the following form:

$$D^{-1}(\mathbf{k}; \mathbf{G}, 0) + \overline{\overline{T}}^{-1}(\mathbf{G}) \frac{\Omega}{i} \sum_{\mathbf{G}'} \Delta A(-\mathbf{G}') D^{-1}(\mathbf{k}; \mathbf{G}', 0) = \overline{\overline{T}}^{-1}(\mathbf{G}) I \delta_{\mathbf{G}, 0}, \quad (24)$$

or what is the same:

$$D^{-1}(\mathbf{k}; \mathbf{G}, 0) + \overline{\overline{T}}^{-1}(\mathbf{G}) \frac{\Omega}{i} \cdot \overline{\overline{C}} = \overline{\overline{T}}^{-1}(\mathbf{G}) I \delta_{\mathbf{G}, 0}, \quad (25)$$

where:

$$\overline{\overline{C}} = \sum_{\mathbf{G}'} \Delta A(-\mathbf{G}') D^{-1}(\mathbf{k}; \mathbf{G}', 0). \quad (26)$$

Multiplying Equation (25) by $\Delta A(-\mathbf{G}')$ and adding the overall reciprocal vectors, \mathbf{G} , the equation needed to determine $\bar{\bar{C}}$ is found:

$$\bar{\bar{C}} + \sum_{\mathbf{G}} \Delta A(-\mathbf{G}) \bar{\bar{T}}^{-1}(\mathbf{G}) \frac{\Omega}{i} \cdot \bar{\bar{C}} = \sum_{\mathbf{G}} \Delta A(-\mathbf{G}) \bar{\bar{T}}^{-1}(\mathbf{G}) \delta_{\mathbf{G},0}, \tag{27}$$

from which, we have:

$$\bar{\bar{C}} + \sum_{\mathbf{G}} \Delta A(-\mathbf{G}) \bar{\bar{T}}^{-1}(\mathbf{G}) \frac{\Omega}{i} \cdot \bar{\bar{C}} = \Delta A(0) \bar{\bar{T}}^{-1}(0), \tag{28}$$

from here:

$$\bar{\bar{C}} = \left[I + \sum_{\mathbf{G}} \Delta A(-\mathbf{G}) \bar{\bar{T}}^{-1}(\mathbf{G}) \frac{\Omega}{i} \right]^{-1} \cdot \Delta A(0) \bar{\bar{T}}^{-1}(0), \tag{29}$$

Substituting this expression for $\bar{\bar{C}}$ in Equation (25), we finally obtain the values for the $D^{-1}(\mathbf{k}; 0, 0)$ matrix block:

$$D^{-1}(\mathbf{k}; 0, 0) = \bar{\bar{T}}^{-1}(0) - \bar{\bar{T}}^{-1}(0) \frac{\Omega}{i} \cdot \left[I + \sum_{\mathbf{G}} \Delta A(-\mathbf{G}) \bar{\bar{T}}^{-1}(\mathbf{G}) \frac{\Omega}{i} \right]^{-1} \cdot \Delta A(0) \bar{\bar{T}}^{-1}(0). \tag{30}$$

Thus, substituting Equation (30) in Equation (6), the value of $A_{eff}(\mathbf{k})$ is obtained:

$$A_{eff}(\mathbf{k}) = i\Omega^{-1} \left\{ \left[\bar{\bar{T}}^{-1}(0) - \bar{\bar{T}}^{-1}(0) \frac{\Omega}{i} \cdot \left[I + \sum_{\mathbf{G}} \Delta A(-\mathbf{G}) \bar{\bar{T}}^{-1}(\mathbf{G}) \frac{\Omega}{i} \right]^{-1} \cdot \Delta A(0) \bar{\bar{T}}^{-1}(0) \right]^{-1} + \begin{bmatrix} 0_3 & K_{3 \times 6}(0, 0) \\ (K_{3 \times 6}(0, 0))^T & 0_6 \end{bmatrix} \right\}. \tag{31}$$

By factoring, we reach the following expression:

$$A_{eff}(\mathbf{k}) = i\Omega^{-1} \left\{ \left[I + \sum'_{\mathbf{G}} \Delta A(-\mathbf{G}) \bar{\bar{T}}^{-1}(\mathbf{G}) \frac{\Omega}{i} \right]^{-1} \cdot \left[I + \sum_{\mathbf{G}} \Delta A(-\mathbf{G}) \bar{\bar{T}}^{-1}(\mathbf{G}) \frac{\Omega}{i} \right]^{-1} \bar{\bar{T}}(0) + \begin{bmatrix} 0_3 & K_{3 \times 6}(0, 0) \\ (K_{3 \times 6}(0, 0))^T & 0_6 \end{bmatrix} \right\}. \tag{32}$$

The apostrophe in the sum indicates that the term $\mathbf{G} = 0$ is excluded. This expression is valid for small-filling fractions; the inversion of the matrix is not too large.

Finally, let us apply Equation (32) to calculate the effective tensors for a phononic crystal in the quasi-static limit ($\mathbf{k} \rightarrow 0, \omega \rightarrow 0$). In this case, from Equation (9), we have:

$$A_{eff}(\mathbf{k} \rightarrow 0) = i\Omega^{-1} \left[I + \sum'_{\mathbf{G}} \Delta A(-\mathbf{G}) \bar{\bar{T}}^{-1}(\mathbf{G}) \frac{\Omega}{i} \right]^{-1} \cdot \left[I + \sum_{\mathbf{G}} \Delta A(-\mathbf{G}) \bar{\bar{T}}^{-1}(\mathbf{G}) \frac{\Omega}{i} \right]^{-1} \bar{\bar{T}}(0). \tag{33}$$

3. Numerical Results and Discussion

In this section, to check the validity of the formulas above, we will calculate the effective parameters in the quasi-static limit for three-dimensional elastic solid-solid phononic crystals with cubic lattice structures. Utilizing the fact that at the long-wavelength limit, the elastic wave that travels through the artificial material does not experience the structure of the materials that constitute it, and the phononic crystal behaves as if it were homogeneous. Hence, the numerical simulations were implemented using Equation (33). The initial procedure for calculating the effective parameters indicated in (33) begins with fixing a low frequency ω and an initial wave vector \mathbf{k}_0 (defined in the long-wavelength regime of the propagation of elastic waves, $\mathbf{k}_0 \rightarrow 0$). In this first iteration, the effective tensors $\bar{\rho}_{eff}(\mathbf{k}_0, \omega)$ and $\bar{S}_{eff}(\mathbf{k}_0, \omega)$ are calculated for the established quasi-static wave vector. It is important to note that our numerical results are calculated by discretizing the inclusion into a small

number of parts, n , and according to its geometry, the value of its form factor $F(\mathbf{G})$ can be introduced in the formulas as a function of the position of its center of gravity and filling fraction in the unit cell of the phononic crystal. This leads to the system defined in (33) for the solution of a system of linear algebraic equations of $9n$ unknowns. Otherwise, the numerical method of the theory developed here gives the effective response of density and stiffness in terms of summations over \mathbf{G} . Our results converged for $N = (41)^3$ summands in the computation (N denotes the number of plane waves) over \mathbf{G} , which allows us to consider a finite number of components for the displacement and stiffness fields in the expansion of plane waves in the phononic crystal. It can be seen that the term $\mathbf{G} = 0$ provides the main contribution to the Fourier expansion, to study the properties of the average field at the long-wavelength limit.

It is important to mention that, in these analytical expressions, when we increase the number of plane waves, a new iteration (i) is realized; then, the effective parameters are recalculated. In this work, this iterative calculation process converged with the following condition of magnitudes for the components of the effective tensor: $\left| \frac{A_{eff,i} - A_{eff,i-1}}{A_{eff,i}} \right| \leq 10^{-5}$; within this limit of convergence, 3–5 iterations were sufficient. With the expressions derived above, our formalism allows us to reduce the size of the system of equations for the calculation of the effective elastic parameters.

In the following scenarios, the unit cell has a lattice parameter of $a = 0.01$ m and for the sake of convenience, we discretize the inclusion in small elements of cubic geometry with an edge ratio of $(1/11)a$; the form factor of the inclusion is calculated by using the following definition:

$$F(\mathbf{G}) = \frac{1}{V_c} \int_{V_{inc}} e^{-i\mathbf{G}r} dr, \tag{34}$$

with V_c (V_{inc}) being the volume of the unit cell (inclusion). Consequently, we find that $F(\mathbf{G})_{cube} = f \frac{\text{sen}(X) \cdot \text{sen}(Y) \cdot \text{sen}(Z)}{X \cdot Y \cdot Z}$, where: $f = \frac{d_x d_y d_z}{V_c}$, $X = \frac{G_x d_x}{2}$, $Y = \frac{G_y d_y}{2}$ and $Z = \frac{G_z d_z}{2}$.

As a first check, we have obtained the effective parameters of a three-dimensional (3D) phononic crystal formed by an inclusion of cubic geometry with an edge of $(7/11)a$, centered in a cubic lattice (see Figure 1).

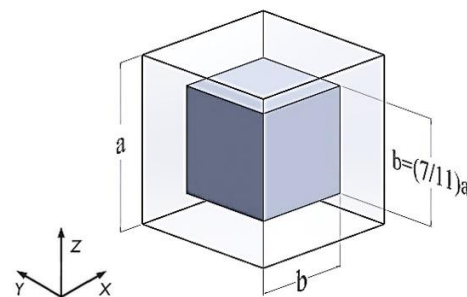


Figure 1. A 3D phononic crystal of a unit-cell cubic form, with a cube inclusion.

Unlike the previously published works, it is interesting in our results that the approach shown here allows us to model periodic structures with materials where the anisotropy in its crystalline symmetry can be different from that in the cubic form. In this case, we will consider an Indium (In) inclusion in an Iron (Fe) matrix corresponding to the tetragonal and cubic symmetries, respectively. The material parameters of Fe are [39]: $\rho_{Fe} = 7870$ kg/m³; the stiffness constants (GPa) are $C_{Fe,11} = 231.4$, $C_{Fe,12} = 134.7$ and $C_{Fe,44} = 116.4$. Meanwhile, those of In are [40]: $\rho_{In} = 7290$ kg/m³; the stiffness constants (GPa) are $C_{In,11} = 45.2$, $C_{In,33} = 44.9$, $C_{In,12} = 40.0$, $C_{In,13} = 41.2$, $C_{In,44} = 6.52$ and $C_{In,66} = 12.0$. For this structure, the fill fraction corresponds to a fixed value of 0.25. The computational results

of Equation (33) for the nonzero elements of the homogenized matrices $\bar{\rho}_{eff}$ (kg/m³) and $\bar{C}_{eff} = \bar{S}_{eff}^{-1}$ (10² GPa) are:

$$\bar{\rho}_{eff} = \begin{pmatrix} 7720.5 & 0 & 0 \\ 0 & 7720.5 & 0 \\ 0 & 0 & 7720.5 \end{pmatrix},$$

and

$$\bar{C}_{eff} = \begin{pmatrix} 1.58 & 0.906 & 0.911 & 0 & 0 & 0 \\ 0.906 & 1.58 & 0.911 & 0 & 0 & 0 \\ 0.911 & 0.911 & 1.570 & 0 & 0 & 0 \\ 0 & 0 & 0 & 0.635 & 0 & 0 \\ 0 & 0 & 0 & 0 & 0.635 & 0 \\ 0 & 0 & 0 & 0 & 0 & 0.685 \end{pmatrix}.$$

According to these results, the 3D solid phononic crystal has a tetragonal symmetry (6 independent values of elastic stiffness constants in \bar{C}_{eff}). The matrix $\bar{\rho}_{eff}$ is isotropic, being characterized by the scalar [3]:

$$\rho_{eff} = \rho_a f + \rho_b(1 - f), \tag{35}$$

which, as has been demonstrated, is the standard average for periodic structures constituted of solid-solid elastic materials.

Another scenario is depicted in Figure 2, showing the geometry of a 3D phononic crystal of a unit-cell cubic form and one centered inclusion in the form of a parallelepiped of *In* in a *Fe* host.

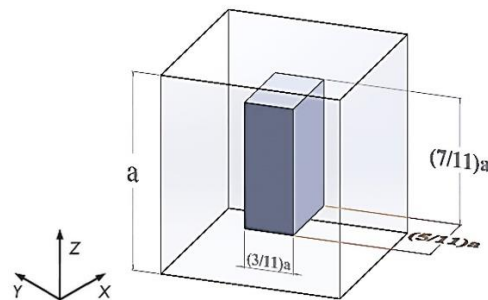


Figure 2. A 3D phononic crystal of a unit-cell cubic form with an inclusion in the form of a parallelepiped.

Here, the filling fraction has a value of 0.078. Thus, from (33), we find that the array of values for the effective density (kg/m³) and stiffness constants matrices (10² GPa) are:

$$\bar{\rho}_{eff} = \begin{pmatrix} 7824.2 & 0 & 0 \\ 0 & 7824.2 & 0 \\ 0 & 0 & 7824.2 \end{pmatrix},$$

and

$$\bar{C}_{eff} = \begin{pmatrix} 2.07 & 1.18 & 1.20 & 0 & 0 & 0 \\ 1.18 & 2.01 & 1.19 & 0 & 0 & 0 \\ 1.20 & 1.19 & 2.09 & 0 & 0 & 0 \\ 0 & 0 & 0 & 0.0962 & 0 & 0 \\ 0 & 0 & 0 & 0 & 1.017 & 0 \\ 0 & 0 & 0 & 0 & 0 & 0.0967 \end{pmatrix}.$$

The effective mass density turns out to be diagonal, and it adjusts to Equation (35) again. On the other hand, the effective stiffness constants exhibit nine independent values that are shown in matrix-form for \bar{C}_{eff} ; therefore, the three-dimensional solid-solid

phononic media behaves like an orthorhombic crystal, which is due to the parallelepiped form of the inclusion.

Now we are going to focus our attention on presenting the computational results for the effective mass density and elastic stiffness tensors of a 3D phononic crystal with a cubic lattice, with a centered inclusion of In in a T-form (not centrosymmetric) of a square cross-section (chosen for computational convenience), where the host material is Fe . The scenario is depicted in Figure 3.

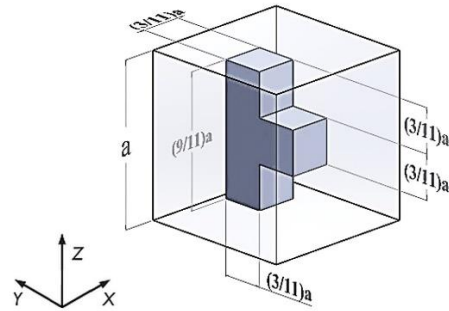


Figure 3. A 3D phononic crystal of a unit-cell cubic form, with an inclusion in a T-form shown in square cross-section.

For this specific design of artificial material, the corresponding filling fraction is 0.081. The corresponding effective parameters values calculated from Equation (33) are:

$$\bar{\rho}_{eff} = \begin{pmatrix} 7822.9 & 0 & 0 \\ 0 & 7822.9 & 0 \\ 0 & 0 & 7822.9 \end{pmatrix},$$

and

$$\bar{C}_{eff} = \begin{pmatrix} 2.057 & 1.198 & 1.185 & 0 & 0 & 0 \\ 1.198 & 2.088 & 1.187 & 0 & 0 & 0 \\ 1.185 & 1.187 & 2.014 & 0 & 0 & 0 \\ 0 & 0 & 0 & 0.959 & 0 & 0 \\ 0 & 0 & 0 & 0 & 0.921 & 0 \\ 0 & 0 & 0 & 0 & 0 & 1.024 \end{pmatrix}.$$

As can be seen, the resulting effective mass density matrix (in kg/m^3) indicates a linear behavior for its three spatial components that shows good agreement with Equation (35), as it is again a periodic structure with solid components. Based on the results provided by the matrix of effective elastic constants (in 10^2 GPa), the homogenized 3D phononic structure presents nine different elastic constants, which indicates that the artificial material has an orthorhombic crystalline anisotropy. Indeed, the anisotropy in the components of the effective elastic stiffness tensor of this structure obeys the form and the relationship of the length of the inclusion in the period of the cubic lattice, along the principal axes, \hat{x} , \hat{y} and \hat{z} (see also the parallelepiped inclusion). It is evident in this non-centrosymmetric inclusion that the anisotropic response will be more noticeable if the filling fraction is increased.

Finally, we present the computational results at the quasi-static limit for the effective elastic compliance constants (\bar{S}_{eff}) of several well-known phononic structures that are composed of isotropic solid materials. The case studies will consist of the individual calculation of a spherical and cubic inclusion in a cubic lattice. The solid phononic material will be composed of steel (bulk modulus (B) = 160 GPa and shear modulus (μ) = 79.3 GPa) [41] in a glass host (B = 40 GPa and μ = 26.2 GPa) [41] for different values of the filling fraction (see Figure 4). Here, the effective parameters were determined by using the following expressions: $S_{11} = (3B + \mu)/(9B\mu)$, $S_{12} = (2S_{11} - S_{44})/2$ and $S_{44} = 1/\mu$. In the case of the spherical inclusion, we use Equation (34); $F(\mathbf{G})_{sphere} = 3f \frac{sen(\mathbf{G}\cdot r_0)}{(\mathbf{G}\cdot r_0)^3} - \frac{cos(\mathbf{G}\cdot r_0)}{(\mathbf{G}\cdot r_0)^2}$, with $f = \frac{4\pi}{3} \frac{r_0^3}{V_C}$, and r_0 is the radius of the sphere.

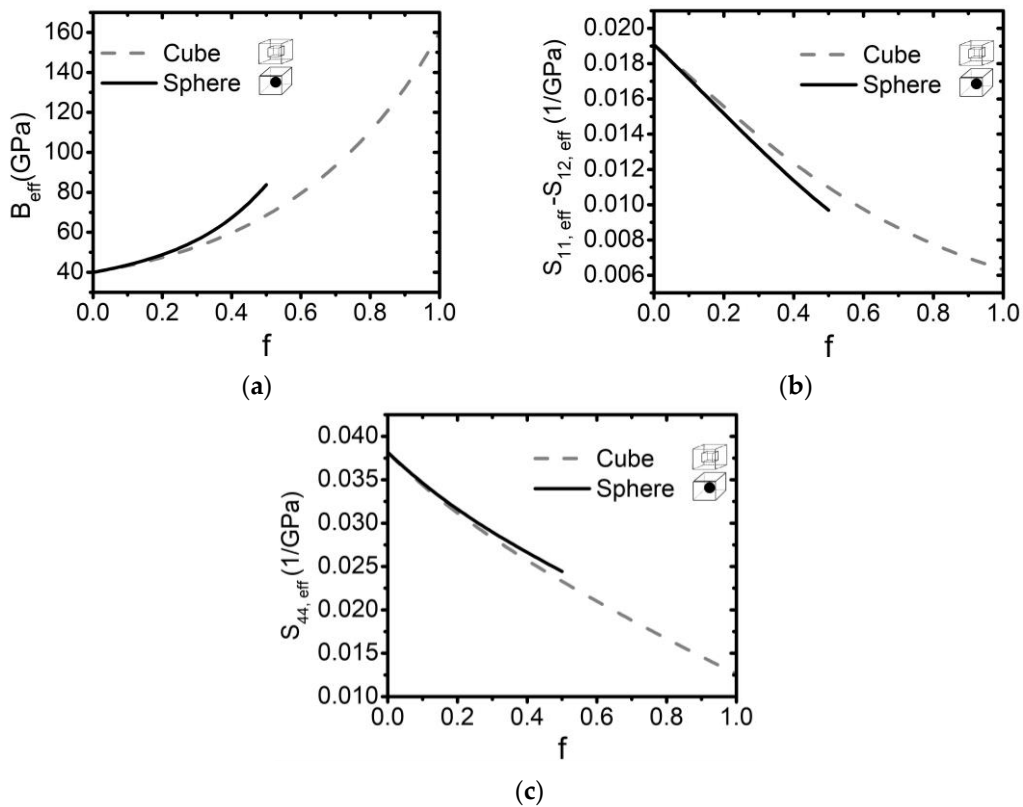


Figure 4. Effective parameters as a function of the filling fraction of a solid-solid 3D phononic crystal for a cubic matrix of glass with cubic and spherical inclusions of steel: (a) B_{eff} ; (b) $S_{11,eff} - S_{12,eff}$, and (c) $S_{44,eff}$.

As f is increased in these high-symmetry structures, note that in the case when the spherical inclusions of the neighboring cells touch each other, the sphere reaches its maximum volume within the unit cell and does not completely fill it; therefore, the fill fraction (V_{inc}/V_c) covers the interval $0 \leq f \leq \frac{\pi}{6}$. This is unlike the scenario of cubic inclusions, where, by touching the inclusions of neighboring cells, the cubes consequently completely fill the unit cell, and f reaches the value of 1.

As verification, we have also compared our results with those of other homogenization theories reported in the literature, considering the quasi-static limit. We have obtained the effective parameters $\bar{\rho}_{eff}$ and \bar{C}_{eff} of a 3D phononic material comprising a prismatic inclusion in a cubic unit cell ($a = 0.01$ m), which represents a typical one-dimensional periodic structure (Figure 5). The inclusion, as in the previous case, is discretized into small cubic elements wherein the form factor is defined by Equation (34). The materials corresponding to the matrix and inclusion are aluminum ($\rho_{Al} = 2700$ kg/m³; the stiffness constants (GPa) are $C_{Al,11} = 106.80$, $C_{Al,12} = 60.70$ and $C_{Al,44} = 28.20$) [42] and silicon ($\rho_{Si} = 2330$ kg/m³; the stiffness constants (GPa) are $C_{Si,11} = 166.00$, $C_{Si,12} = 63.90$ and $C_{Si,44} = 79.60$) [42], respectively.

The effective parameters obtained by this approach using the discretization of the inclusion are presented by points in Figure 6 (see panels (a)–(d)). Solid, dotted, and dashed lines indicate the effective values obtained in the long-wavelength regime, using the theories for laminated composite materials developed in previous studies [38,43,44] (e.g., the conventional homogenization theory and asymptotic homogenization). As can be seen in the graphs, the results obtained by the approximation presented here have good agreement with the other calculations at the filling fractions indicated.

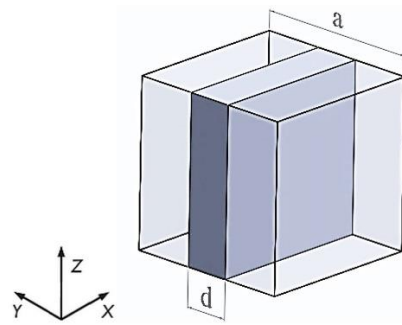


Figure 5. A cubic unit cell with an inclusion in the form of a plate (one-dimensional phononic crystal).

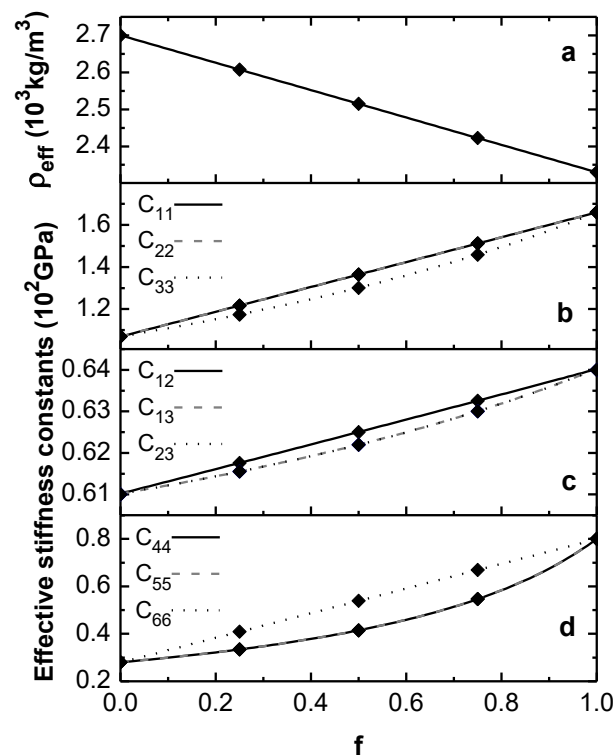


Figure 6. Comparison of the calculation of the effective parameters $\bar{\rho}_{eff}$ and \bar{C}_{eff} obtained in the quasi-static limit for a one-dimensional phononic crystal. The lines correspond to the results obtained by other homogenization theories, while the dots indicate the values obtained by this inclusion discretization approach. There is a good agreement between the calculations.

These results allow us to explain and analyze the anisotropy of homogenized three-dimensional elastic phononic crystals as a function of the crystal symmetry of their constituents and any shape of the inclusions in the unit cell.

4. Conclusions

The results demonstrate that three-dimensional solid phononic crystals can be considered as a homogeneous anisotropic medium in the low-frequency limit. The approach presented here is efficient and provides accurate calculations of the effective parameters, specifically the stiffness tensor and mass density. Numerical simulations show a dependence in terms of summations over the vectors of the reciprocal lattice, by discretizing the inclusion volume into small parts (small cubes). Particularly for three-dimensional solid-solid phononic crystals composed of *In* inclusions in a *Fe* host with fixed values of the filling fraction in a cubic lattice, it was observed that anisotropy is found in the rigidity and is associated with the Bravais lattice of the materials that constitute it and of the geometry of the inclusion, e.g., for a cube inclusion, the homogenized phononic

crystal behaved as a tetragonal material, unlike the parallelepiped and T-form inclusions, which exhibited orthorhombic crystal symmetry. Moreover, the effective density $\bar{\rho}_{eff}$ of solid-solid composites at the quasi-static (long-wavelength) limit is isotropic linear in form and depends on f . This relationship does not apply to composite structures with a fluid matrix. Besides this, our method can be extended to study high-symmetry structures versus the inclusion fill fraction (e.g., spherical and cubic inclusion in a cubic lattice composed of isotropic solid materials). Finally, as a check, for a one-dimensional phononic crystal, our results show good agreement with other homogenization theories reported in the literature. In conclusion, the examples and results shown here will be useful for the design of metamaterials with predetermined elastic properties.

Author Contributions: Conceptualization, J.F.M., A.M.-S., M.A.M.M. and M.M.M.; methodology, J.F.M., R.C.A.L. and J.A.L.-L.; software, J.F.M., A.C.P.R., M.A.M.M. and F.S.C.; validation, J.F.M., F.S.C., A.H.H.J. and J.A.L.-L.; writing—original draft preparation, J.F.M.; A.C.P.R. and A.H.H.J.; writing—review and editing, J.F.M., A.M.-S., M.M.M., J.A.L.-L., F.S.C., R.C.A.L. and A.C.P.R.; supervision, J.F.M., F.S.C., A.H.H.J. and J.A.L.-L. All authors have read and agreed to the published version of the manuscript.

Funding: This research received no external funding.

Acknowledgments: This work was partially supported by UPAEP.

Conflicts of Interest: The authors declare no conflict of interest.

References

- Hashin, Z.; Shtrikman, S. A Variational Approach to the Theory of the Effective Magnetic Permeability of Multiphase Materials. *J. Appl. Phys.* **1962**, *33*, 3125. [[CrossRef](#)]
- Milton, G.W. Bounds on the Electromagnetic, Elastic, and Other Properties of Two-Component Composites. *Phys. Rev. Lett.* **1981**, *46*, 542. [[CrossRef](#)]
- Berryman, J.G. Long-wavelength propagation in composite elastic media I. Spherical inclusions. *J. Acoust. Soc. Am.* **1980**, *68*, 1809. [[CrossRef](#)]
- Sheng, P.; Callegri, A.J. Differential effective medium theory of sedimentary rocks. *Appl. Phys. Lett.* **1984**, *44*, 738. [[CrossRef](#)]
- Kushwaha, M.S.; Halevi, P.; Dobrzynski, L.; Djafari, R. Acoustic band structure of periodic elastic composites. *Phys. Rev. Lett.* **1993**, *71*, 2022. [[CrossRef](#)]
- Ni, Q.; Cheng, J. Long wavelength propagation of elastic waves in three-dimensional periodic solid-solid media. *J. Appl. Phys.* **2007**, *101*, 073515. [[CrossRef](#)]
- Ni, Q.; Cheng, J.-C. Homogenization of Three-Dimensional Periodic Solid-Solid Elastic Composites. *Chin. Phys. Lett.* **2007**, *24*, 747–750.
- Zhou, X.-W.; Zou, X.-Y.; Wang, T.-H.; Cheng, J.-C. Effective velocity of 2D phononic crystals with rectangular lattice. *Ultrasonics* **2010**, *50*, 577–582. [[CrossRef](#)]
- Liu, J.; Wu, Y.; Li, F.; Zhang, P.; Liu, Y.; Wu, J. Anisotropy of homogenized phononic crystals with anisotropic material. *Europhys. Lett.* **2012**, *98*, 36001. [[CrossRef](#)]
- Flores Méndez, J.; Salazar Villanueva, M.; Ambrosio Lázaro, R.C.; Calixto Sirene, B.; Mota González, M.L.; Candia García, F. Plane Wave-Perturbative Method for Evaluating the Effective Speed of Sound in 1D Phononic Crystals. *Adv. Mater. Sci. Eng.* **2016**, *2016*, 3017835. [[CrossRef](#)]
- Krokhin, A.A.; Arriaga, J.; Gumen, L.N. Speed of Sound in Periodic Elastic Composites. *Phys. Rev. Lett.* **2003**, *91*, 264302. [[CrossRef](#)] [[PubMed](#)]
- Kafesaki, M.; Penciu, R.S.; Economou, E.N. Air Bubbles in Water: A Strongly Multiple Scattering Medium for Acoustic Waves. *Phys. Rev. Lett.* **2000**, *84*, 6050. [[CrossRef](#)] [[PubMed](#)]
- Cervera, F.; Sanchis, L.; Sánchez-Pérez, J.V.; Martínez-Sala, R.; Rubio, C.; Meseguer, F.; López, C.; Caballero, D.; Sánchez-Dehesa, J. Refractive Acoustic Devices for Airborne Sound. *Phys. Rev. Lett.* **2002**, *88*, 023902. [[CrossRef](#)] [[PubMed](#)]
- Mei, J.; Liu, Z.; Wen, W.; Sheng, P. Effective Mass Density of Fluid-Solid Composites. *Phys. Rev. Lett.* **2006**, *96*, 024301. [[CrossRef](#)] [[PubMed](#)]
- Torrent, D.; Håkansson, A.; Cervera, F.; Sánchez-Dehesa, J. Homogenization of Two-Dimensional Clusters of Rigid Rods in Air. *Phys. Rev. Lett.* **2006**, *96*, 204302. [[CrossRef](#)]
- Torrent, D.; Sánchez-Dehesa, J. Anisotropic mass density by two-dimensional acoustic metamaterials. *New J. Phys.* **2008**, *10*, 023004. [[CrossRef](#)]
- Laude, V.; Iglesias Martínez, J.A.; Wang, Y.F.; Kadic, M. Effective anisotropy of periodic acoustic and elastic composites. *J. Appl. Phys.* **2021**, *129*, 215106. [[CrossRef](#)]

18. Li, J.; Chan, C.T. Double-negative acoustic metamaterial. *Phys. Rev. E* **2004**, *70*, 055602(R). [[CrossRef](#)]
19. Dong, H.W.; Zhao, S.D.; Wei, P.; Cheng, L.; Wang, Y.S.; Zhang, C. Systematic design and realization of double-negative acoustic metamaterials by topology optimization. *Acta Mater.* **2019**, *172*, 102–120. [[CrossRef](#)]
20. Wang, T.; Wang, L.M.; Ma, Z.D.; Hulbert, G.M. Elastic analysis of auxetic cellular structure consisting of re-entrant hexagonal cells using a strain-based expansion homogenization method. *Mater. Des.* **2018**, *160*, 284–293. [[CrossRef](#)]
21. Yuan, S.Q.; Shen, F.; Bai, J.M.; Chu, C.K.; Wei, J.; Zhou, K. 3D soft auxetic lattice structures fabricated by selective laser sintering: TPU powder evaluation and process optimization. *Mater. Des.* **2017**, *120*, 317–327. [[CrossRef](#)]
22. Hou, S.Y.; Li, T.T.; Jia, Z.; Wang, L.F. Mechanical properties of sandwich composites with 3d-printed auxetic and non-auxetic lattice cores under low velocity impact. *Mater. Des.* **2018**, *160*, 1305–1321. [[CrossRef](#)]
23. Eringen, A.C. *Microcontinuum Field Theories I: Foundations and Solids*, 1st ed.; Springer: New York, NY, USA, 1999.
24. Duan, S.Y.; Wen, W.B.; Fang, D.N. A predictive micropolar continuum model for a novel three-dimensional chiral lattice with size effect and tension-twist coupling behavior. *J. Mech. Phys. Solids* **2018**, *121*, 23–46. [[CrossRef](#)]
25. Kaczmarczyk, L.; Pearce, C.J.; Bicanic, N. Studies of Microstructural Size Effect and Higher-order Deformation in Second-order Computational Homogenization. *Comput. Struct.* **2010**, *88*, 1383–1390. [[CrossRef](#)]
26. Reis, F.D.; Ganghoffer, J.F. Construction of micropolar continua from the asymptotic homogenization of beam lattices. *Comput. Struct.* **2012**, *112–113*, 354–363. [[CrossRef](#)]
27. Dirrenberger, J.; Forest, S.; Jeulin, D.; Colin, C. Homogenization of periodic auxetic materials. *Procedia Eng.* **2011**, *10*, 1847–1852. [[CrossRef](#)]
28. Ha, C.S.; Hestekin, E.; Li, J.H.; Plesha, M.E.; Lakes, R.S. Controllable thermal expansion of large magnitude in chiral negative Poisson's ratio lattices. *Phys. Status Solidi B* **2015**, *252*, 1431–1434. [[CrossRef](#)]
29. Tian, Y.; Zhang, W.; Tan, Z.; Cho, C. Chiral edge states for phononic crystals based on shunted piezoelectric materials. *Extrem. Mech. Lett.* **2022**, *50*, 101568. [[CrossRef](#)]
30. Chen, Y.; Frenzel, T.; Guenneau, S.; Kadic, M.; Wegener, M. Mapping acoustical activity in 3D chiral mechanical metamaterials onto micropolar continuum elasticity. *J. Mech. Phys. Solids* **2020**, *137*, 103877. [[CrossRef](#)]
31. Airoidi, A.; Bettini, P.; Zazzarini, M.; Scarpa, F. Failure and energy absorption of plastic and composite chiral honeycombs. *WIT Trans. Built Environ.* **2012**, *126*, 101–114.
32. Mohammad, M.; Amanul, S.; Behnam, A.; Barthelat, F. Toughness by segmentation: Fabrication, testing and micromechanics of architected ceramic panels for impact applications. *Int. J. Solids Struct.* **2019**, *158*, 52–65.
33. Ma, Y.H.; Scarpa, F.; Zhang, D.Y.; Zhu, B.; Chen, L.L.; Hong, J. A nonlinear auxetic structural vibration damper with metal rubber particles. *Smart Mater. Struct.* **2013**, *22*, 084012. [[CrossRef](#)]
34. Baravelli, E.; Ruzzene, M. Internally resonating lattices for bandgap generation and low-frequency vibration control. *J. Sound Vib.* **2013**, *332*, 6562–6579. [[CrossRef](#)]
35. Huang, K.X.; Shui, G.S.; Wang, Y.Z.; Wang, Y.S. Elastic wave scattering by a pair of parallel semi-infinite cracks in mechanical metamaterials with multi resonators. *Int. J. Fract.* **2021**, *232*, 199–212. [[CrossRef](#)]
36. Huang, K.X.; Shui, G.S.; Wang, Y.Z.; Wang, Y.S. Enhanced Fracture Resistance Induced by Coupling Multiple Degrees of Freedom in Elastic Wave Metamaterials with Local Resonators. *J. Elast.* **2021**, *144*, 33–53. [[CrossRef](#)]
37. Huang, K.X.; Shui, G.S.; Wang, Y.Z.; Wang, Y.S. Discrete scattering and meta-arrest of locally resonant elastic wave metamaterials with a semi-infinite crack. *Proc. R. Soc. A* **2021**, *477*, 20210356. [[CrossRef](#)]
38. Flores-Méndez, J.; Pérez-Rodríguez, F. Metasolid with anisotropic mass density. *Europhys. Lett.* **2013**, *103*, 54001. [[CrossRef](#)]
39. Rayne, J.A.; Chandrasekhar, B.S. Elastic Constants of Iron from 4.2° to 300° K. *Phys. Rev.* **1961**, *122*, 1714. [[CrossRef](#)]
40. Chandrasekhar, B.S.; Rayne, J.A. Elastic Constants of Indium from 1.4° to 300°K. *Phys. Rev.* **1961**, *124*, 1011. [[CrossRef](#)]
41. Crandall, S.H.; Dahl, N.C.; Lardner, T.J.; Sivakumar, M.S. *An Introduction to the Mechanics of Solids (In SI Units)*, 3rd ed.; Tata McGraw Hill Education Private Limited: Nueva Delhi, India, 2012; p. 259.
42. Kittel, C. *Introduction to Solid State Physics*, 8th ed.; Wiley: New York, NY, USA, 2004; pp. 21–84.
43. Castellero, J.B.; Otero, J.A.; Ramos, R.R.; Bourgeat, A. Asymptotic homogenization of laminated piezocomposite materials. *Int. J. Solids Struct.* **1998**, *35*, 527–541. [[CrossRef](#)]
44. Bravo-Castillero, J.; Rodríguez-Ramos, R.; Mechkour, H.; Otero, J.A.; Cabanas, J.H.; Sixto, L.; Sabina, F.J. Homogenization and effective properties of periodic thermomagneto-electroelastic composites. *J. Mech. Mater. Struct.* **2009**, *4*, 819–836. [[CrossRef](#)]